A unified smoke control method based on signed distance field

Abstract

Smoke control involves shape and path. A unified framework able to deal with both of them will enable animators to manipulate the shape and path of smoke animation more effectively. In this paper, we develop such a unified framework. With our approach, path control, shape control, and mixed control of both can be handled satisfactorily in the same framework. In order to develop this framework, we use a signed distance field to provide three control forces: path control force, boundary control force, and shape control force based on medial axis point clouds. The path control force makes the smoke move along the appointed route, the boundary control force keeps the smoke moving through specified regions only, and the shape control force enables the smoke to form various given shapes. The boundary control force and the shape control force are two novel control forces developed in this paper. To make the smoke form the target shape more accurately, we develop an adaptive strategy to adjust the divergence field. We also employ a new hybrid vortex particle scheme to enhance the turbulence flow details. The examples given in this paper indicate that our proposed framework is advantageous over the existing shape control approaches and path control algorithms, and a naive combination of the two.

Keywords: smoke animation, control algorithm, shape control, path control, mixed control.

1. Introduction

The special effects industry has witnessed a greater emphasis on the use of physically-based fluid animation to reproduce realistic fluid effects. Besides realism, the ability to control the fluid behavior is also very important and challenging. Smoke control is an important topic of fluid control. It has drawn the attention of many researchers, and some control algorithms for special effects simulation have been developed. These algorithms can be roughly classified into two groups: path control and shape control. Path control algorithms enable smoke to follow given paths, and shape control methods make smoke form the target shapes.

Since smoke control involves both shape and path, a unified framework able to tackle both of them will enable animators to manipulate the shape and path of smoke animation more effectively. Such a unified framework has not been developed, and the work carried out in this paper indicates that it cannot be achieved by a simple combination of the existing shape control methods and path control algorithms, even with the modifications given in Section 4 of this paper.

In order to address this issue, we propose a unified control algorithm to integrate shape control, path control, and mixed control into the same framework. Our control algorithm translates 3D surface geometry models and space curves representing paths into a signed distance field. Through the signed distance field, we provide two novel control forces: boundary control force and shape control force based on medial axis point clouds. The boundary control force restricts the smoke to the appointed regions, and the shape control force is used to drive the smoke into given shapes. In addition, we use the path control force presented by Kim *et al.* [1]. In order to improve the accuracy of shape control, we developed an adaptive strategy for divergence field adjustment. By combining the vortex particle method [2] and the Langevin particle method [3] together, we design a hybrid vortex particle scheme to enhance the turbulent flow details. This hybrid vortex particle can freely switch between two identities of vortex particles and Langevin particles depending on its spatial location.

The contributions of our work include: (a) a unified control framework, which integrates path control, shape control, and mixed control of both, (b) two new control forces, i.e., the boundary force restricting the smoke to appointed regions and the shape control force making the smoke form target shapes, (c) an adaptive strategy for the divergence field adjustment used in the shape control, (d) a hybrid vortex particle scheme to enhance turbulent flow details.

Our approach gives a solution to the problem of mixed control of shape and path which has not been addressed by the existing approaches. With our proposed approach, the shape and path of smoke animation can be controlled more effectively.

The rest of the paper is organized as follows. Section 2 provides a brief overview of previous related work. In Section 3, the adopted algorithm is elaborated. Section 4 presents the experimental results. Finally in Section 5, the conclusion of the present work is drawn and a proposal for future work is given.

2. Related work

In 1997, Foster and Metaxas [4] introduced embedded controllers which enable animators to control fluid movement. Based on this algorithm, Foster and Fedkiw [5] proposed one modified algorithm, in which 3D parametric space curves are sampled to generate oriented points, and the velocity of these local points is further modified to control fluid movement. Three years later, Rasmussen *et al.* [6] presented a control algorithm based on particles, which were set accordingly to generate either hard or soft control to achieve user desired animation effects. Pighin *et al.* [7] introduced a new representation, radial basis functions carried by moving particles, to express fluids, and modified the moving track of particles to realize the control of fluid. Schpok *et al.* [8] proposed another algorithm which automatically extracts simulation features like vortices and uniform advection, and enabled users to manipulate and modify these features to realize fluid animation control. In addition, other researchers such as Angelidis *et al.* [9, 10], and Weißssmann *et al.* [11] all used smoke control algorithms based on vortex filaments and rings. All the above studies provided a direct control algorithm, but failed in making the fluid form target shapes or follow specified paths.

In order to solve this problem, Treuille *et al.* [12] developed a control algorithm based on user-specified keyframes, which determines control forces through a continuous quasi-Newton optimization. By applying this algorithm, they succeeded in making smoke form any possible target shape. However, this approach is time-consuming. Therefore, Mc-Namara *et al.* [13] further improved it by adopting an adjoint method. Unfortunately, the adjoint method still requires much computation and storage. Although directly exerting a control force on fluids without considering optimization fails to ensure the fluid form a target shape at a specific moment in time, it is enforced in an easy manner and saves much computation expense as indicated in the existing literature, notably those by Fattal *et al.* [14], Hong and Kim [15], Shi and Yu [16, 17]. Similar to these research studies, we also developed several control forces to make the fluid match various targets. Since the scaling parameter and the direction of our control forces do not change over time, their computation can be performed only once in the whole simulation process. As the magnitude of our control forces is merely dependent on the smoke density, the additional cost for our control forces shown in Table 1 and discussed in Section 4 of this paper is very small. Next to the algorithms based on Eulerian approaches [14, 15, 16, 17], particle based Lagrangian methods, such as smooth particle hydrodynamics (SPH) introduced by Desbrun and Gascuel [18], are also very popular in computer graphics. Thürey *et al.* [19] used control particles based on SPH to drive fluid to a target shape while preserving small fluid details. The work focuses more on liquid rather than smoke. Liu *et al.* [20] proposed a cloud shape control method based on the ellipsoidal-blob approximations of 3D models. Compared to shape control, path control has not been addressed so much by researchers. Credit in this field goes to Kim *et al.* [1], who achieved path control of smoke animation by using a linear feedback control method. We are unaware of any work which integrates shape control and path control to obtain smoke animation. In this paper, we will address this issue.

3. Algorithm

Developed from Eulerian approaches, our control algorithm consists of two parts, pre-computation and simulation loop. First, we introduce the basic fluid solver in Subsection 3.1. Next, we investigate the precomputation in Subsection 3.2 with a main focus on the calculations of the signed distance field and the scaling parameter, and the determination of the direction of our control forces. Finally, we discuss the simulation loop in Subsection 3.3.

3.1. Basic fluid solver

The incompressible Navier-Stokes equations can be written as:

$$\mathbf{u}_t + (\mathbf{u} \cdot \nabla)\mathbf{u} + \frac{\nabla p}{\rho} = \mu \nabla^2 \mathbf{u} + \mathbf{f}, \tag{1}$$

$$\nabla \cdot \mathbf{u} = 0, \tag{2}$$

where $\mathbf{u}$ is the fluid velocity, p is the pressure, ρ is the fluid density and μ is the viscosity. The term $\mathbf{f}$ represents external forces including gravity, buoyancy, and our three control forces: the boundary control force, the shape control force based on medial axis point clouds, and the path control force. In order to determine the unknowns such as pressure and velocity in the above fluid equations, Equations 1 and 2 are discretized on a regular Cartesian grid by applying the staggered MAC-grid arrangement for unknowns like pressure and velocity. We employ the methods presented in references [21] and [22] to solve equations 1 and 2.

3.2. Precomputation

Precomputation includes determination of the signed distance field and the three control forces. Since the signed distance field is a prerequisite of determining the three control forces, we investigate it first.

3.2.1. Computation of signed distance field

As discussed above, our fluid control can be divided into shape control, path control and mixed control of shape and path. The signed distance field is different for different fluid controls. Therefore, we will discuss below how to determine the signed distance field for each of the three controls.

For shape control, we load CG models, adopt the signed distance computing method proposed by Bærentzen *et al.* [23], and obtain the following signed distance function:

$$\phi_{shape}(\mathbf{x}) = \begin{cases} -d_t(\mathbf{x}) & if\ \mathbf{x}\ is\ inside\ the\ model, \\ d_t(\mathbf{x}) & otherwise, \end{cases} \tag{3}$$

where $d_t(\mathbf{x})$ expresses the shortest Euclidean distance from the spatial point to the triangle meshes constituting the target shape. Note that, the CG model must be a closed mesh.

For path control, our algorithm uses a NURBS curve to represent the curve constraining the bulk flow path, which is similar to [1] and can be written as:

$$\mathbf{x} = C(l), \quad l \in [0, 1] \tag{4}$$

where l is the parameter coordinate. By setting the path influence radius R_f, we can further develop a signed distance function $\phi_{path}(\mathbf{x})$ as below:

$$\phi_{path}(\mathbf{x}) = d_c(\mathbf{x}) - R_f, \tag{5}$$

where $d_c(\mathbf{x})$ is the shortest distance from the spatial point to the curve $C(l)$.

Finally, if animators want to achieve mixed control of shape and path, the algorithms introduced above for shape control and path control can be employed to compute the signed distance functions $\phi_{shape}(\mathbf{x})$ and $\phi_{path}(\mathbf{x})$, respectively. The signed distance function $\phi_{mixed}(\mathbf{x})$ for mixed control is determined below.

The signed distance function $\phi_{mixed}(\mathbf{x})$ will be used to determine the boundary control force which pulls the smoke that is outside the path influence region and/or the target shape back inside. According to equations 3 and 5, when the smoke is outside both the path influence region and the target shape, $\phi_{shape}(\mathbf{x})$ and $\phi_{path}(\mathbf{x})$ are positive. If the smoke is closer to the target shape than the path influence region, the smoke should be moved to the target shape. Accordingly, the signed distance function $\phi_{mixed}(\mathbf{x})$ should be taken to be $\phi_{shape}(\mathbf{x})$ which is smaller than $\phi_{path}(\mathbf{x})$. If the smoke is closer to the path influence region than the target shape, the smoke should be moved to the path influence region and $\phi_{mixed}(\mathbf{x})$ should be taken to be $\phi_{path}(\mathbf{x})$ which is smaller than $\phi_{shape}(\mathbf{x})$. Considering these two situations, we obtain the following equation used to determine the signed distance function $\phi_{mixed}(\mathbf{x})$:

$$\phi_{mixed}(\mathbf{x}) = \min(\phi_{shape}(\mathbf{x}), \phi_{path}(\mathbf{x})). \tag{6}$$

The signed distance function $\phi_{mixed}(\mathbf{x})$ is only C^0 continuous. The directions of our boundary control forces may be discontinuous when we compute them from $\phi_{mixed}(\mathbf{x})$. However, it doesn't make the solver instable since we use the unconditionally stable semi-Lagrangian method [21] to solve the advection equation.

3.2.2. Computation of our control forces

Three control forces are introduced to control smoke movement. Each of them is determined by the product of the smoke density, the scaling parameter and the direction of the control force. In what follows, we will elaborate them.

Boundary control force: We provide a new boundary control force as:

$$\mathbf{f}_{boundary} = \begin{cases} \rho \frac{|\phi(\mathbf{x})|}{dx}\left(-\frac{\nabla\phi(x)}{\|\nabla\phi(x)\|}\right) & if\ \phi(\mathbf{x}) > 0, \\ 0 & otherwise, \end{cases} \tag{7}$$

where $\phi(\mathbf{x})$ can be either $\phi_{path}(\mathbf{x})$ or $\phi_{shape}(\mathbf{x})$, or even $\phi_{mixed}(\mathbf{x})$, dx is the length of the grid cell which is used to achieve a more effective control effect, i.e., the smoke within a higher resolution region is more difficult to deviate from the target shape due to the action of a bigger boundary control force caused by a smaller dx, $\frac{|\phi(\mathbf{x})|}{dx}$ is the scaling parameter, and $(-\frac{\nabla\phi(x)}{\|\nabla\phi(x)\|})$ is the normalized direction of boundary control force. In equation 7 and the following equations, ρ is the smoke density which is the same as the one in equation 1.

Our boundary control force is applied in the region where $\phi(\mathbf{x}) > 0$, i.e. outside the target shape and the path radius. According to the definition $\frac{|\phi(\mathbf{x})|}{dx}$, the farther the smoke drifts away from the target shape or the more it deviates from the control path, the larger the boundary control force. Our proposed boundary control force is similar to but different from

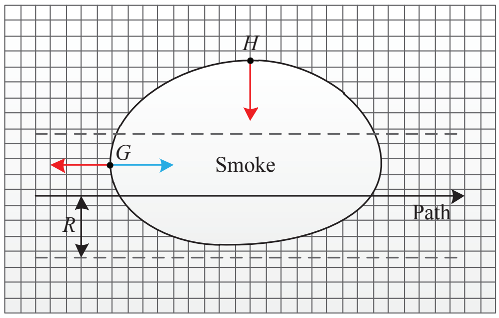

Figure 1: Conflict between the shape feedback force and the path control force at point G. The red and blue arrows respectively represent the directions of the shape feedback force and the path control force.

the shape feedback force introduced by Shi and Yu [17]. Although both control forces depend on a signed force field, the shape feedback force in [17] cannot be used in path control directly since it may block the movement of the smoke particles along the path. As shown in Fig. 1, H and G are two points on the smoke boundary, and the red arrows indicate the shape feedback force on them. H is located out of the path influence area, and the shape feedback force on it points to the negative gradient direction of the signed distance function of the path influence area, which is orthogonal to the path. This is also what we expect from the shape feedback force: to pull the smoke deviating from the target path back to the path influence area. G is located within the path influence area, and the shape feedback force on it points to the gradient direction of the signed distance function of the smoke. However, as we see in Fig. 1, the shape feedback force at G is in the opposite direction to the path control force, which is presented by the blue arrow.

Due to such problems incurred by the shape feedback force, we modified it to develop our boundary control force, which is imposed not on the smoke boundary but on the region excluding the target path influence area and target shape. Its direction only depends on the signed distance functions of the target shape and the target path. This arrangement produces two advantages. Firstly, the boundary control force manages to act independently of the path control force, as there is no boundary control force in the path influence area, and no impact on the smoke's movement along the path thereafter. Secondly, in contrast to the direction of the shape feedback force, which needs to be calculated in every simulation step, the direction of our boundary control force will not change over time, so that the calculation is performed only once in the whole simulation, saving additional cost of the control algorithms.

Shape control force based on medial axis point clouds: To make the smoke form a specified shape, it is not enough to only use the boundary control force. Here, we introduce another new shape control force based on medial axis point clouds. After computing the signed distance field of the target shape, we extract the medial axis point clouds using the Lapla-

(a) Results from using our shape control force

(b) Results from using the adaptive geometric potential method [17]

Figure 2: Comparison between our shape control force and the adaptive geometric potential method [17] in shape control.

cian criteria as Xia *et al.* did in [24]. Our shape control force is defined as follows:

$$\mathbf{f}_{medial} = \begin{cases} \rho S(\frac{d_p(\mathbf{x})}{R_w})G(\mathbf{x}) & if\ \phi_{shape}(\mathbf{x}) \le 0, \\ 0 & otherwise, \end{cases} \tag{8}$$

where $d_p(\mathbf{x})$ denotes the distance from grid points to the medial axis points, R_w indicates the influence radius of the medial axis points. Since medial axis points are not equally distributed, a large influence radius will lead to more smoke in the area with more medial axis points but less smoke in the region with fewer medial axis points. In order to avoid this artifact caused by excessive mutual interference among medial axis points, the influence radius R_w should be set small so that the smoke can be exclusively subject to the shape control force derived from the medial axis points nearby. In our examples we set R_w to cover two grid cells. $G(\mathbf{x})$ stands for the direction of the shape control force. If $\mathbf{x}$ is the grid point location, $\mathbf{y}$ is the medial axis point location, then $G(\mathbf{x}) = \frac{\mathbf{y}-\mathbf{x}}{\|\mathbf{y}-\mathbf{x}\|}$. It should be noted that the shape control force is actually a resultant force. When we compute the shape control force at a grid point, we need to find out all the medial axis points whose influence radius covers this grid point. For each of these medial axis points, we obtain a control force using equation 8. Then the resultant shape control force at this grid point is determined by superimposing all these control forces. The scaling parameter $S(m)$ is a step function defined by:

$$S(m) = \begin{cases} 3m^2 - 2m^3 & if\ 0 \leqslant m \leqslant 1, \\ 0 & otherwise, \end{cases} \tag{9}$$

$S(m)$ increases monotonically in the interval [0,1]. Within the influence radius of the medial axis points, the farther a grid point is away from a medial axis point, the larger the shape control force acting at the grid point, and vice versa.

Our proposed shape control force is different from and advantageous over the adaptive geometric potential proposed by Shi and Yu in [17]. The adaptive geometric potential in [17] is based on skeletons around which the smoke is gathered. In contrast, our proposed shape control force is based on medial axis point clouds which cover many more areas than skeletons, gathering the smoke around every medial axis point. Therefore, our proposed shape control force allows the smoke to spread more efficiently in the target shape. What is more, we set our shape control force in such a way that the farther the smoke is from the medial axis point, the larger the force, thus the smoke can be dragged in more easily by those medial axis points at the deeper ends of the long and narrow areas, making the resulting shape fully formed. Besides, extracting the medial point clouds is much easier than extracting skeletons.

(a) The resulting shape from our proposed method (b) The resulting shape from Shi and Yu's method

Figure 3: Comparison between the resulting shape from our method and that from the method in [17].

In order to support the above discussions, we have used our proposed shape control force and the adaptive geometric potential method introduced in [17] to generate a bunny shape depicted in Figures 2 and 3, and made a comparison between them. In the figures, Fig. 2(a) and Fig. 3(a) are created from our proposed shape control force, and Fig. 2(b) and Fig. 3(b) are created with the adaptive geometric potential method. It can be clearly seen that the final bunny shape in Fig. 2(a) created with our proposed shape control force matches the target shape much better than that in Fig. 2(b) generated with the adaptive geometric potential method. Such a difference can be more clearly observed in Fig. 3 especially in the bunny's ears. Due to the dragging action of the medial axis points, 100% of the bunny shape shown in Fig. 3(a) is filled with the smoke driven by our proposed shape control force. In contrast, only 89.5% of the bunny shape is filled with the smoke controlled by the adaptive geometric potential method introduced in [17]. Some long and narrow areas such as the bunny's ears, are not filled as shown in Fig. 3(b) since the control force produced by the method gathers smoke around the skeleton which cannot drive the smoke spread into long and narrow regions.

Path control force: According to the tangent field used in [1], we provide a path control force as follows:

$$\mathbf{f}_{path} = \begin{cases} \rho S(1 - \frac{d_c(\mathbf{x})}{R_f})T(\mathbf{x}) & if\ \phi_{path}(\mathbf{x}) \leq 0, \\ 0 & otherwise, \end{cases} \tag{10}$$

where $T(\mathbf{x})$ is a unit tangent vector of the path which represents the direction of the path control force, and the scaling parameter S is as defined in equation 9.

3.3. Simulation loop

After the precomputation processing, we will perform the simulation loop. Apart from adding our control forces and solving the Navier-Stokes equations, we also employ our hybrid vortex particles and a divergence field adjustment during the simulation loop. They will be explained next.

Algorithm 1

1: Add the boundary control force;
2: Add the shape control force if needed;
3: Add the path control force if needed;
4: Enhance the turbulence flow details using hybrid vortex particles;
5: Solve the advection equation with the Semi-Lagrangian method;
6: Adjust the divergence field if needed;
7: Solve pressure equation to ensure fluid incompressibility;
8: Advect the hybrid vortex particles and update the vorticities of particles if needed;
9: Advect the density field;
10: Seed hybrid vortex particles if needed;

3.3.1. Algorithm flow

The pseudo-code of the whole simulation loop is listed in Algorithm 1.

3.3.2. Hybrid vortex particle

During the control of smoke movement, it is also desirable to generate abundant turbulence details. We present a hybrid vortex particle method which makes vortex particles [2] and Langevin particles [3] work together to create more details in the controlled flow.

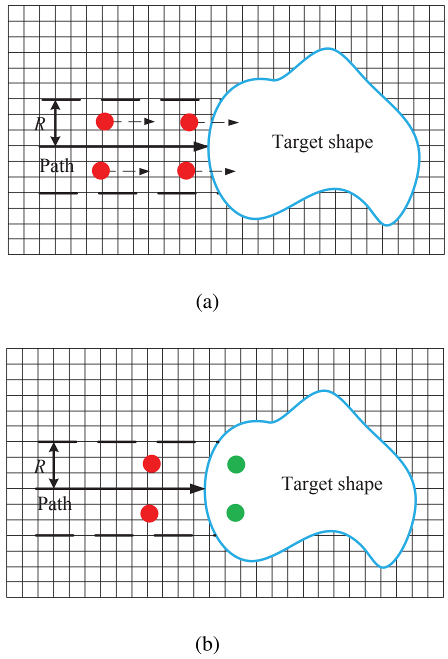

Figure 4: Dual identities of hybrid vortex particles. Red and green points all stand for hybrid vortex particles among which the red ones have the identity of Langevin particles, and the green ones possess the identity of vortex particles, and the dashed arrows show the trajectory of each hybrid vortex particle. Fig. 4(a) indicates the old locations and identity of the hybrid vortex particles, and Fig. 4(b) shows the new locations and identities of these hybrid vortex particles in the next moment.

Both the vortex particle method and the Langevin particle method are efficient and easy to use. These methods provide a vorticity force computed by particles and add it into the external force term in the Navier-Stokes equations. The difference between them is that the Langevin particles do a better job in path control, while the vortex particles are superior to the Langevin particles in shape control. Figures 5 and 6 clearly demonstrate the strengths and weaknesses of both particles.

In Fig. 5, we compared path control by using a slash as the target path and generating three sets of examples with different enhancements. The original flow without any enhancement is shown in Fig. 5(a), the enhanced flow by the Langevin particles is demonstrated in Fig. 5(b), and that by the vortex particles is indicated in Fig. 5(c). It can be observed that the motion of the smoke is closer to the original flow when we use the Langevin particles, whereas the smoke is dispersed by the vorticity forces produced by vortex particles and deviates from the path. This is mainly because the Langevin particle method succeeded in agitating the flow directly in relation to the mean flow path which does not exist in the vortex particle method.

In Fig. 6, we made a comparison of shape control between the Langevin particle method and the vortex particle method. It is observed that the target shape is formed more quickly and the smoke looks more turbulent when we use the vortex particles

(a) Original flow

(b) Langevin particle method

(c) Vortex particle method

Figure 5: Comparison between Langevin particle method and vortex particle method in path control.

(a) Langevin particle method

(b) Vortex particle method

Figure 6: Comparison between langevin particle method and vortex particle method in shape control.

to enhance the turbulence details. The reason for this is that the turbulence energy injected by the vortex particles can be initialized by users at the last step of Algorithm 1, whereas that injected by the Langevin particles depends on the dissipation of turbulence structures. If the dissipation is very small in some locations, the injected turbulence energy there would also be small.

Therefore, in order to enhance turbulence flow details freely for both path control and shape control, we combine the advantages of the two particles in developing our hybrid vortex particles, which switches between the two identities depending on their spatial location. As shown in Fig. 4(a), when a hybrid particle is located within the influence region of the path, we label it as a Langevin particle and inject turbulence energy in the same way as the Langevin particle method. On the contrary, when a hybrid particle is inside the region of the target shape, we label it as a vortex particle, as shown in Fig. 4(b). By utilizing our hybrid vortex particle, we can enhance turbulence flow details freely for both path control and shape control.

3.3.3. Divergence field adjustment

The volume of smoke is sometimes larger than the target shape during the shape control. Therefore, it is difficult to make all the smoke move into the target shape because of the incompressibility of the fluid. As a result, the smoke will not form the target shape faithfully, especially when the target shape is detailed. In order to simulate the expansion of gaseous combustion products, Feldman *et al.* [25] proposed directly adjusting the fluid's divergence field. Inspired by their work, we adjust the divergences of some fluid cells inside the target shape to make the smoke contract so that the smoke outside the target shape is able to move in. The divergence for each fluid cell is:

$$\nabla \cdot \mathbf{u} = \varphi. \tag{11}$$

We choose some medial axis points which are near the center of the target shape. Then we adjust the divergences of the fluid cell where each medial axis point lies and its eight surrounding cells. In these cells, φ should be less than 0 to reduce the excess smoke. The smaller the value of the divergence adjustment, the faster the smoke is reduced. In our examples, we set the value to -1. For all other cells, the value of φ is set to 0. To enforce equation 11, we changed the Poisson's equation into:

$$\nabla^2 p = \frac{\rho}{\Delta t}(\nabla \cdot \mathbf{u} - \varphi). \tag{12}$$

Contraction means reduction of the smoke. In order to prevent the smoke from disappearing, we cannot perform the contraction all the time. To address this problem, we developed an adaptive strategy for the divergence field adjustment. First, we count the number n_g of the grid points inside the target shape. Second, in each simulation step, we check the number n_i of the grid points filled with smoke inside the target shape. Third, we calculate the smoke filling percentage $s_p = n_i/n_g$. If the smoke filling percentage equals the threshold T_1, we perform the adjustment of the divergence field as described above. If the smoke filling percentage is less than the threshold T_2, we stop adjusting the divergence field to make it incompressible. T_1 and T_2 are two parameters specified by the user. Our experiments indicate that when $T1 = 100\%$ and $T2 = 99.5\%$, satisfactory results are produced. In addition, we use a density threshold T_d to decide whether a grid point is filled with smoke or not. If the density of a grid point is larger than T_d, it is filled with smoke. For all the examples given in this paper, we set $T_d = 0.01$. Fig. 9 shows the results before and after the divergence field adjustment for the dragon model. We can see that a more detailed dragon is formed by employing our adaptive adjustment strategy.

In [14], Fattal *et al.* also used a smoke gathering term to improve the resulting shape. It operates by making the smoke density inside the target shape higher than that outside the target shape, so that the resulting shape can be easily identified as the target. However, after the target shape is formed, there is still some smoke left outside the target shape. If the target shape has some small features, the smoke outside the target shape would blur them, leaving an indistinct and ambiguous contour. As shown in Fig.10, the resulting shape from the target-driven method lacks details and makes its contour appear blurred. In

Figure 7: Limitation of the smoke gathering term in [14]. We use the bunny model as the target shape and add some smoke source at the beginning of the simulation. Then we implement the smoke gathering term and it can be observed that the bunny look like emerging from an amorphous static cloud of smoke.

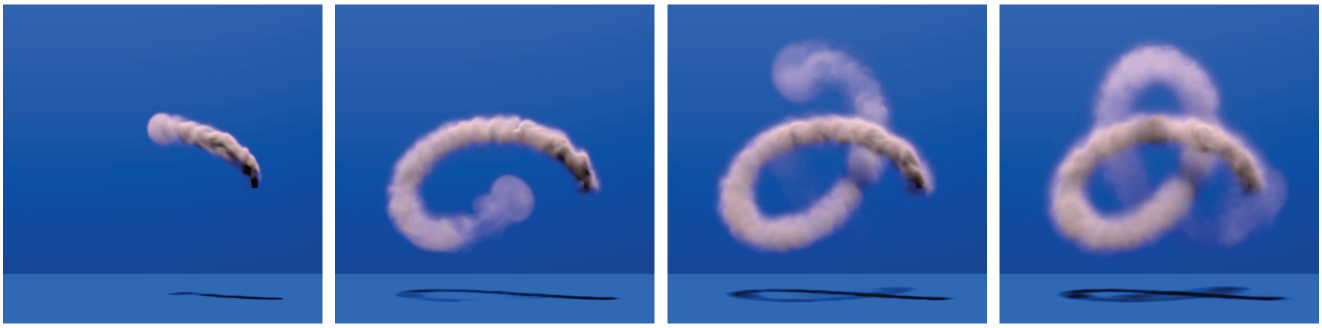

Figure 8: Path control with the knot model.

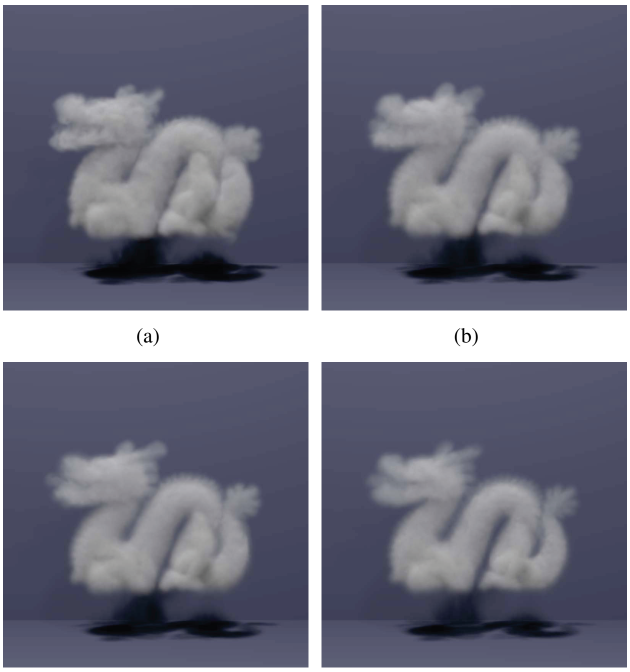

(a) (b)

(c) (d)

Figure 9: The divergence field adjustment used in the shape control of the dragon model. (a). Before the divergence field adjustment. (b) Five frames after performing the divergence field adjustment. (c). Ten frames after performing the divergence field adjustment. (d). Twenty frames after performing the divergence field adjustment.

contrast, our resulting shape is more detailed and clearer, which is depicted around the dragon's horns, tail, and bone spurs on the back. This improvement comes from our divergence field adjustment, which removes the smoke inside the target shape, making room for the smoke outside to move in. Moreover, the smoke gathering technique can lead to artifacts, making the target shape appear to have emerged directly from a static amorphous smoke cloud as shown in Fig. 7. This artifact cannot be observed in our examples.

4. Results and Discussions

We have implemented our algorithm on a PC with Intel Core i5 CPU 3.20 GHz and 4GB RAM. The PBRT library [26] was employed to render the volume data with material density and the NURBS++ library [27] was used to manipulate NURBS curves.

Fig. 8 shows four frames of our path control for the knot model. The resolution of the simulation grid is $128 \times 128 \times 128$. We set the path radius to 0.03. The whole precomputation process lasts $201s$. A hybrid vortex particle is sampled every two steps at the smoke source to enhance the turbulence details.

Using a dragon model as the target shape and taking the grid resolution to be $128 \times 128 \times 128$, we have compared our proposed shape control method with the target-driven method introduced in [14] by Fatal and Lischinski, and depicted the obtained results in Figures 11 and 10 where Figures 11(a) and 10(a) are from our proposed shape control method, and Figures 11(b)

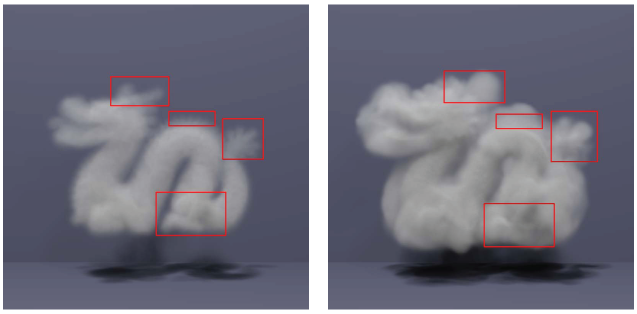

(a) Our resulting shape (b) Fattal and Lischinski's resulting shape

Figure 10: Comparison between the resulting shapes given in Fig. 11.

and 10(b) are from the target-driven method introduced by Fatal and Lischinski.

The whole precomputation process using our proposed shape control method takes 135s. In order to enhance turbulence details, we randomly chose the initial positions of hybrid vortex particles to be some medial axis points which are not so close to each other. We sample these hybrid vortex particles just once at the beginning and assign them a lifetime. When the presence of the particles exceeds its lifetime, they are deleted automatically.

In Figures 11 and 10, we observe that our method can provide more detail, especially around the dragon's tail and bone spurs on the back etc. which were highlighted in Fig. 10. The improvement made by our proposed method comes from our divergence field adjustment strategy, which removes the smoke inside the target shape, making room for the smoke outside to move in. Such a treatment makes the resulting shape more detailed and clearer. In contrast, the smoke gathering algorithm introduced by Fattal and Lischinski cannot do the same job as our divergence field adjustment.

By making smoke move along the designated path and form the shape of a bunny at the same time, we demonstrated the mixed control of both shape and path using our proposed unified framework, and examined whether the combination of the methods given in [1] and [14] can complete the same task.

For the proposed unified framework, the grid resolution is taken to be $64 \times 64 \times 64$, and the path radius is set to 0.04. At intervals of every 2 simulation steps, we positioned one hybrid vortex particle respectively at the start and end of the path. The obtained result is given in Fig. 12(a). The precomputation process takes 70s.

In order to test whether or not the combination of existing methods can do the same job as our proposed unified framework, we combined the path control method given in [1] with the shape control algorithm introduced in [14] as elaborated in Appendix A of this paper and tested the feasibility of such a combination. Fig. 12(b) gives the result obtained from the combined control algorithm. It can be seen that when the target shape is formed, more and more smoke overflows from the path influence area and the target shape due to the incompressibility. However, the overflowing smoke deviates more and more from the target path and target shape. This is mainly because both the driving force and the normal force are restricted within their influence areas. When the smoke moves outside the influence areas of both forces there is no way to pull it back.

The most direct method to solve the above problem is to increase the influence areas of the driving force and the normal force so that the smoke outside the path influence area and the target shape can be pulled back, but due to the conflicting action of the driving force and the normal force described in Appendix A, this measure does not actually work. Another simple way is to reduce the smoke source in the simulation. The result obtained from this measure is depicted in Fig. 12(c). Although the problem shown in Fig. 12(b) was alleviated, the target bunny shape cannot be created since there is not enough smoke.

From the above discussion, it is clear that combining the path control method in [1] with the shape control method in [14] even with further modifications to the combination, can not achieve the mixed control of shape and path. Our proposed framework successfully solves this problem and the mixed control algorithm can be used to manipulate both the shape and path of smoke animation effectively. Firstly, our boundary control force is able to restrict the smoke motion within the appointed regions including not only the path influence area but also the target shape. Therefore, it can be regarded as a combination of the driving force and the normal force, and also succeeds in avoiding the conflict as discussed in Appendix A. Due to these reasons, it can be imposed on the entire region apart from the target shape and the path influence area. Secondly, our divergence field adjustment strategy can eliminate excess smoke when the target shape is formed.

In order to further demonstrate the effectiveness of our proposed framework in the mixed control, we presented a more complicated example in Fig. 13. For this example, the smoke first forms the shape of a teddy. Then it is forced to go through a hollow ring in the middle. Finally, it drops on to the ground to take the shape of a kangaroo. The grid resolution is $128 \times 128 \times 128$, and the path radius is 0.03. The precomputation took 375s. The sampling strategy for the hybrid vortex particles was divided into two steps. In the first step, where we made the smoke form the shape of teddy, we sampled the hybrid vortex particles as we did for Fig. 11(a). In the second step, where we forced the smoke to go through the hollow ring in the middle, and finally form the shape of a kangaroo, we deleted all the hybrid vortex particles sampled in the first step and resampled them as we did for Fig. 12(a). The mixed control demonstrated in Fig. 12(a) and Fig. 13 has not been seen in previous algorithms. Our method helps to create more interesting animations.

The computations of the scaling parameter and the direction of our control forces will all be completed during the precomputation process. In the simulation stage, our control forces can be quickly obtained by combining the scaling parameter and the directions of these control forces with the density values at grid points through simple multiplication. Therefore, the time used to determine our control forces is very small compared to that spent on the simulation. This is clearly demonstrated by the data in Table 1 where the third column gives the average time per frame spent on the simulation, the fourth column presents

(a) Our shape control method

(b) The target-driven method proposed by Fattal and Lischinski

Figure 11: Comparison between our control algorithm and the target-driven method proposed by Fattal and Lischinski.

(a) Our control method

(b) Combination of the methods given in [1] and [14]

(c) Combination of the methods given in [1] and [14] with less smoke source

Figure 12: Comparison between our control algorithm and the combination of the methods given in [1] and [14] for a mixed control.

Figure 13: Mixed control example (II): smoke first forms the shape of a teddy, then is controlled to go through the hollow ring in the middle, and finally drops on the ground taking the shape of a kangaroo.

the time used to determine the control forces, and the fifth column is the percentage of the time used for our control forces over the average time spent on the simulation, which represents the additional cost of smoke animation. Obviously, the additional cost for our control algorithm is very small. Compared with the additional cost of 15% and 10% for fluid control mentioned in [14] and [17] respectively, ours is more economical with a percentage of no more than 3%.

Thanks to parallelism, our computation of control forces can be further accelerated by using a GPU. Moreover, our control algorithm is based on a unified framework, which enables the operations of both path control and shape control. In contrast, most previous algorithms managed exclusively either shape control (as addressed by Treuille *et al.* [12]; McNamara *et al.* [13]; Fattal *et al.* [14]; Hong and Kim [15]; Thürey *et al.* [19]; Shi and Yu [16, 17]) or path control (as investigated by Kim *et al.* [1]). As demonstrated in Fig. 12 and Fig. 13, mixed control can be achieved by our algorithm so that the diversified needs of animators can be easily met.

5. Conclusions

In this paper, we have presented a novel unified technique to control the dynamics of shape-constrained smoke based on signed distance fields without direct manipulation of simulation parameters. In order to develop the unified technique, we have proposed two novel control forces: the boundary control force and the shape control force based on medial axis point clouds. A signed distance field has been used to provide these two control forces and the path control force. The combined application of these three forces effectively drives smoke to follow a given path and/or form a required target shape. We also presented an adaptive strategy to adjust the divergence field and introduced a new hybrid vortex particle scheme to enhance the details of turbulence flow for the creation of more accurate shapes.

We have made some comparisons between our proposed unified framework and existing approaches. By comparing our proposed mixed control algorithm with the combination of the path control method in [1] and shape control method in [14], we concluded that our proposed framework can manipulate both the shape and path of smoke animation effectively, whereas the combination of the methods in [1] and [14] cannot do the job.

A number of examples have been presented to demonstrate the applications of our proposed technique in controlling smoke animation. These application examples indicate: 1). our proposed technique can use the same framework to achieve path control, shape control, and mixed control of both path and shape which has not been reported in previous algorithms, 2). the produced results retain the realism and nuances of smoke animation. In addition, our proposed technique provides animators with more convenience and enables them to achieve both shape control and path control in smoke animation, and can be applied in liquid control as well since the mathematical expressions of our control forces have the same form as those for liquid con-

Table 1: Performance comparison.

Examples	Grid size	Time for simulation per step	Time for computing control forces	Percentage
Fig. 8	$128 \times 128 \times 128$	$24.9s$	$0.308s$	1.24%
Fig. 11	$128 \times 128 \times 128$	$25.4s$	$0.337s$	1.33%
Fig. 12	$64 \times 64 \times 64$	$2.4s$	$0.058s$	2.42%
Fig. 13	$128 \times 128 \times 128$	$26.5s$	$0.508s$	1.92%

trol.

Our approach has the following limitations. The first one is that the smoke may not look alive in the latter part of the simulation process, especially for the shape control. This is due to the joint effect of the boundary control force and the divergence field adjustment. Because we employ the boundary control force, the smoke outside the target shape is pushed into the shape. If the volume of the smoke is larger than the target shape, the divergence field adjustment is used to eliminate excessive smoke. As a result, the smoke inside the target shape will reach an equilibrium state. To address this issue, we will develop an adaptive strategy so that the time and magnitude of the boundary control force will be determined according to the target shape formation situation. The second limitation is the reduction of the smoke caused by the divergence field adjustment. To fix this problem, a more elaborate adaptive strategy combined with additional smoke sources should be developed.

In the future, we will extend this work to animated shapes and paths. In this case, since the scaling parameter and the direction of the control forces will change over time, we should try to make use of the coherence between animated shapes and paths to reduce the computational cost. We will also extend this algorithm to the interaction between fluids and other objects while keeping the smoke dynamics.

Appendix A.

The target velocity field designed in [1] by Kim *et al.* to control the smoke is a superposition of four velocity components. In order to combine it with the target-driven method introduced in [14] properly, we transformed these velocity components into corresponding control forces. Unfortunately, there is a conflict when applying all these control forces since the driving force obtained from [14] drives the smoke into the target shape and the normal force derived from [1] constrains the smoke motion along the path point at different directions. This conflict can be effectively demonstrated by the blue driving force and red normal force acting at points D and E in Fig. A.14. When the smoke passes point D, it should be pulled back by the normal force to follow the target path. However, the driving force will make it further deviate from the target path. When the smoke reaches point E, it should be dragged into the target shape by the driving force. Since the normal force acts in a different direction, the smoke cannot be moved to the position where it should be. In order to prevent the control force and normal force from interfering with each other, the simplest way is to reduce the respective influence areas of the two control

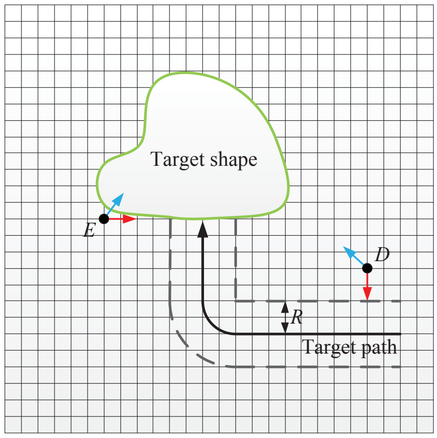

Figure A.14: Conflict between the control forces when combining the methods proposed in [1] and [14]. At points D and E, the blue and red arrows respectively represent the directions of the driving force in [14] and the normal field in [1] which can be considered as a normal force.

forces. The smaller the overlap influence area of the two control forces, the less conflict it causes. The influence area of the driving force is determined by the support radius of the Gaussian blurring filter. The normal force's influence area depends on the magnitude of the normal field radius. In the experiment, we set the support radius of the Gaussian blurring filter and the normal field radius both to cover 5 grid cells. The grid resolution is $64 \times 64 \times 64$, the same as that used in Fig. 12(a) by our unified framework. Since our focus is to figure out whether the above combination method can achieve the mixed control rather than improve the visual effects, we have made little effort to enhance the turbulence flow details. Therefore, the rankine field and the vortex field in [1] are not taken into consideration in the combination method.

References

[1] Kim Y, Machiraju R, Thompson D. Path-based control of smoke simulations. In: Proceedings of the 2006 ACM SIGGRAPH/Eurographics symposium on Computer animation. SCA '06; Aire-la-Ville, Switzerland, Switzerland: Eurographics Association. ISBN 3-905673-34-7; 2006, p. 33–42.

[2] Selle A, Rasmussen N, Fedkiw R. A vortex particle method for smoke, water and explosions. ACM Trans Graph 2005;24(3):910–4.

[3] Chen F, Zhao Y, Yuan Z. Langevin particle: A self-adaptive lagrangian primitive for flow simulation enhancement. Comput Graph Forum 2011;30(2):435–44.

[4] Foster N, Metaxas D. Controlling fluid animation. In: Proceedings of the

1997 Conference on Computer Graphics International. CGI '97; Washington, DC, USA: IEEE Computer Society; 1997, p. 178.
[5] Foster N, Fedkiw R. Practical animation of liquids. In: Proceedings of the 28th annual conference on Computer graphics and interactive techniques. SIGGRAPH '01; New York, NY, USA: ACM. ISBN 1-58113-374-X; 2001, p. 23–30.
[6] Rasmussen N, Enright D, Nguyen D, Marino S, Sumner N, Geiger W, et al. Directable photorealistic liquids. In: Proceedings of the 2004 ACM SIGGRAPH/Eurographics symposium on Computer animation. SCA '04; Aire-la-Ville, Switzerland, Switzerland: Eurographics Association. ISBN 3-905673-14-2; 2004, p. 193–202.
[7] Pighin F, Cohen JM, Shah M. Modeling and editing flows using advected radial basis functions. In: Proceedings of the 2004 ACM SIGGRAPH/Eurographics symposium on Computer animation. SCA '04; Aire-la-Ville, Switzerland, Switzerland: Eurographics Association. ISBN 3-905673-14-2; 2004, p. 223–32.
[8] Schpok J, Dwyer W, Ebert DS. Modeling and animating gases with simulation features. In: Proceedings of the 2005 ACM SIGGRAPH/Eurographics symposium on Computer animation. SCA '05; New York, NY, USA: ACM. ISBN 1-59593-198-8; 2005, p. 97–105.
[9] Angelidis A, Neyret F. Simulation of smoke based on vortex filament primitives. In: Proceedings of the 2005 ACM SIGGRAPH/Eurographics symposium on Computer animation. SCA '05; New York, NY, USA: ACM. ISBN 1-59593-198-8; 2005, p. 87–96.
[10] Angelidis A, Neyret F, Singh K, Nowrouzezahrai D. A controllable, fast and stable basis for vortex based smoke simulation. In: Proceedings of the 2006 ACM SIGGRAPH/Eurographics symposium on Computer animation. SCA '06; Aire-la-Ville, Switzerland, Switzerland: Eurographics Association; 2006, p. 25–32.
[11] Weißssmann S, Pinkall U. Filament-based smoke with vortex shedding and variational reconnection. ACM Trans Graph 2010;29(4):1–12.
[12] Treuille A, McNamara A, Popović Z, Stam J. Keyframe control of smoke simulations. ACM Trans Graph 2003;22(3):716–23.
[13] McNamara A, Treuille A, Popović Z, Stam J. Fluid control using the adjoint method. ACM Trans Graph 2004;23(3):449–56.
[14] Fattal R, Lischinski D. Target-driven smoke animation. In: ACM SIGGRAPH 2004 Papers. SIGGRAPH '04; New York, NY, USA: ACM; 2004, p. 441–8.
[15] Hong JM, Kim CH. Controlling fluid animation with geometric potential: Research articles. Comput Animat Virtual Worlds 2004;15(3-4):147–57.
[16] Shi L, Yu Y. Controllable smoke animation with guiding objects. ACM Trans Graph 2005;24(1):140–64.
[17] Shi L, Yu Y. Taming liquids for rapidly changing targets. In: Proceedings of the 2005 ACM SIGGRAPH/Eurographics symposium on Computer animation. SCA '05; New York, NY, USA: ACM. ISBN 1-59593-198-8; 2005, p. 229–36.
[18] Desbrun M, Cani MP. Smoothed particles: A new paradigm for animating highly deformable bodies. In: Boulic R, Hégron G, editors. Eurographics Workshop on Computer Animation and Simulation, EGCAS '96, August, 1996. Poitiers, France: Springer; 1996, p. 61–76. Published under the name Marie-Paule Gascuel.
[19] Thürey N, Keiser R, Pauly M, Rüde U. Detail-preserving fluid control. In: Proceedings of the 2006 ACM SIGGRAPH/Eurographics symposium on Computer animation. SCA '06; Aire-la-Ville, Switzerland, Switzerland: Eurographics Association. ISBN 3-905673-34-7; 2006, p. 7–12.
[20] Liu S, Jin X, Wang CC, Hui K. Ellipsoidal-blob approximation of 3d models and its applications. Computers & Graphics 2007;31(2):243 –51.
[21] Stam J. Stable fluids. In: Proceedings of the 26th annual conference on Computer graphics and interactive techniques. SIGGRAPH '99; New York, NY, USA: ACM Press/Addison-Wesley Publishing Co. ISBN 0-201-48560-5; 1999, p. 121–8.
[22] Bridson. R. Fluid Simulation for Computer Graphics. Natick, MA, USA.: A. K. Peters, Ltd.; 2008.
[23] Bærentzen JA, Aanaes H. Signed distance computation using the angle weighted pseudonormal. IEEE Transactions on Visualization and Computer Graphics 2005;11(3):243–53.
[24] Xia H, Tucker PG. Distance solutions for medial axis transform. In: Proceedings of the 18th International Meshing Roundtable. Springer Berlin Heidelberg; 2009, p. 247–65.
[25] Feldman BE, O'Brien JF, Arikan O. Animating suspended particle explosions. ACM Trans Graph 2003;22(3):708–15.
[26] Pharr M, Humphreys G. Physically based rendering : from theory to implementation. 2nd ed. Morgan Kaufmann; 2010,.
[27] Lavoie P. The nurbs ++ package. http://libnurbs.sourceforge.net; 2002,.